J. Fluid Mech. (1996), vol. 321, pp. 189–216

The influence of wall cooling on hypersonic boundary-layer separation and stability

By K. W. CASSEL[1], A. I. RUBAN[2] AND J. D. A. WALKER[1]

[1]Department of Mechanical Engineering and Mechanics, Lehigh University, 19 Memorial Drive West, Bethlehem, PA 18015, USA

[2]Department of Mathematics, University of Manchester, Oxford Road, Manchester M13 9PL, UK

(Received 3 April 1995 and in revised form 26 March 1996)

The effect of wall cooling on hypersonic boundary-layer separation near a compression ramp is considered. Two cases are identified corresponding to the value of the average Mach number $\bar{M}$ across the upstream boundary layer approaching the compression ramp. The flow is referred to as supercritical for $\bar{M} > 1$ and subcritical for $\bar{M} < 1$. The interaction is described by triple-deck theory, and numerical results are given for both cases for various ramp angles and levels of wall cooling. The effect of wall cooling on the absolute instability described recently by Cassel, Ruban & Walker (1995) for an uncooled wall is of particular interest; a stabilizing effect is observed for supercritical boundary layers, but a strong destabilizing influence occurs in the subcritical case. Wall cooling also influences the location and size of the separated region. For supercritical flow, progressive wall cooling reduces the size of the recirculating-flow region, the separation point moves downstream, and upstream influence is diminished. In contrast for the subcritical case downstream influence is reduced with increased cooling. In either situation, a sufficient level of wall cooling eliminates separation altogether for the ramp angles considered. The present numerical results closely confirm the strong wall cooling theory of Kerimbekov, Ruban & Walker (1994).

1. Introduction

Triple-deck theory has provided a clear understanding of the viscous–inviscid interactions that occur in a wide variety of flows. The supersonic triple-deck problem was first formulated by Stewartson & Williams (1969) and Neiland (1969), who showed how the presence of a disturbance within a supersonic boundary layer could be transmitted upstream. Triple-deck analysis has subsequently been applied to many problems spanning the full range of flow speeds from subsonic to hypersonic. The formulation was subsequently extended to hypersonic flow with significant wall cooling by Neiland (1973) and later by Brown, Cheng & Lee (1990). Wall cooling is often necessary in hypersonic flow applications in order to combat the high temperatures generated near the surface (Towend 1991; Walberg 1991).

In this study, the problem depicted schematically in figure 1 is of interest, wherein a multilayer structure develops as a hypersonic boundary layer encounters a compression ramp having an asymptotically small ramp angle. Inclusion of the effects of significant wall cooling brings about three primary changes in the hypersonic triple-deck formulation as compared to the classical supersonic problem. The first effect is

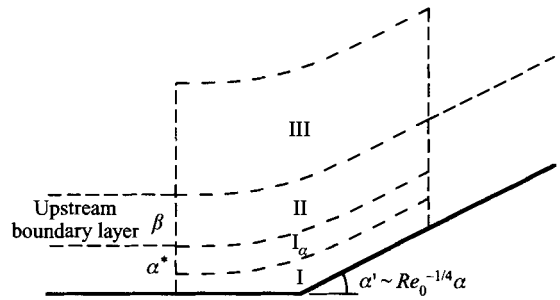

FIGURE 1. Schematic of the triple-deck structure for hypersonic flow over a cold wall near a compression ramp (not to scale).

an overall reduction in the length scales of the triple-deck structure as the surface is progressively cooled (see §2). Secondly, as illustrated in figure 1, the approach boundary layer upstream of the interaction region bifurcates into two layers; now an inner wall layer is required in order to adjust the relatively high boundary-layer temperatures to that of the cold surface. The thickness of the upstream wall layer (region α^*) is much greater than that of the viscous sublayer in the interaction region (region I), and this necessitates an intermediate layer (region I_α) between the conventional viscous sublayer (region I) and the main deck (region II). The intermediate layer is essentially a continuation of the upstream inner wall layer into the interaction region and communicates changes between the viscous sublayer and the main and upper decks; however, it does not contribute to leading order to the displacement effect of the boundary layer (Kerimbekov, Ruban & Walker 1994).

The third and most significant effect of wall cooling consists of a reduction in both the longitudinal extent of the interaction region and the displacement thickness of the viscous sublayer; the former change may come into play even when the mainstream Mach number M_∞ is finite. As shown by Seddougui, Bowles & Smith (1991), wall cooling in subsonic and supersonic flows, where M_∞ is $O(1)$, can shrink the interaction region to such an extent that the characteristic longitudinal length becomes comparable to the thickness of the unperturbed upstream boundary layer; consequently, the upper deck of the triple-deck structure merges with the middle deck and pressure variations across the main portion of the boundary layer become significant. However, such a merger is not possible in a hypersonic flow ($M_\infty \gg 1$) since, even for extremely low wall temperatures, the longitudinal extent of the interaction region is M_∞ times larger than the thickness of the upstream boundary layer. At the same time, this does not mean that the interaction process remains unaffected; indeed, along with the reduction in the displacement thickness contribution due to the viscous sublayer, there is a corresponding rise in the relative contribution from the main deck and both become important to leading order once the wall temperature is sufficiently low. As shown by Neiland (1973), the displacement thickness attributable to the main deck is proportional to the pressure rise induced by the boundary layer. If the average Mach number $\bar{M}$ across the upstream boundary layer is less than one, a pressure increase leads to boundary-layer thickening in the interaction region; on the other hand, if $\bar{M} > 1$, a pressure increase leads to a decrease in the boundary-layer thickness. The former case was referred to as subcritical and the latter as supercritical by Neiland (1973) because of an analogous behaviour for subsonic and supersonic mainstream flows, respectively.

If δ_s and δ_m denote the contributions to displacement thickness in the interaction

zone associated with the sublayer and main deck, respectively, it is evident that there are at least three regimes of interest, namely (1) $\delta_s \gg \delta_m$; (2) $\delta_s \sim \delta_m$ and (3) $\delta_s \ll \delta_m$. Regime 1 corresponds to situations with moderate wall temperatures (such as the adiabatic wall temperature), and from this regime each of regimes 2 and 3 is reached in turn by progressively lowering the temperature of the wall. The first regime is described by the classical triple-deck formulation for supersonic flow (Stewartson & Williams 1969; Neiland 1969), and numerical solutions have been obtained previously by Rizzetta, Burggraf & Jenson (1978), Ruban (1978), Smith & Khorrami (1991) and Cassel, Ruban & Walker (1995) for a boundary layer encountering a compression ramp with various small ramp angles. These results show that a separation zone develops near the corner for ramp angles greater than a certain critical value. As the ramp angle is increased, the extent of the separation region grows, and a plateau forms in the pressure distribution downstream of the separation point. Cassel *et al.* (1995) show that at a second (and larger) critical ramp angle, a streamwise velocity profile develops an inflection point in the recirculation region and the boundary-layer flow eventually becomes unstable; the instability is manifest in the form of a wave packet which grows but remains stationary near the corner for all ramp angles above the second critical value. Note that the instability was only observed when sufficiently refined numerical grids were used.

The third regime is characterized by very low wall temperatures where the displacement-thickness contribution due to the main deck is dominant. This situation has been considered recently by Kerimbekov *et al.* (1994) for subcritical and supercritical boundary layers that encounter a compression ramp. For the limiting case of strong supercritical wall cooling, it was found that there are no disturbances upstream of the corner, and separation can only occur on the inclined portion of the ramp; furthermore, the boundary layer on the ramp exhibits marginal separation behaviour similar to that which is known to occur near the leading edge of thin airfoils at a critical angle of attack (Ruban 1981, 1982 and Stewartson, Smith & Kaups 1982). On the other hand, for strong subcritical wall cooling, the pressure is almost constant downstream of the corner and separation can only occur upstream of the corner. For this case, a Goldstein (1948) singularity occurs at separation, but the theory of Smith & Daniels (1981) may be utilized to continue the solution downstream of the separation point. Further details of the strong wall cooling case are described in §3.

The present calculations were carried out in regime 2 (moderately cooled walls) in order to provide a bridge between existing theories for moderate wall temperatures (regime 1) and strongly cooled walls (regime 3). This parameter range will subsequently be defined more precisely in terms of the wall temperature. The present results for the compression ramp show that wall cooling has a significant effect on both separation and the instability observed by Cassel *et al.* (1995). Wall cooling was found to either stabilize or destabilize the flow depending on whether the flow was supercritical or subcritical, respectively. In addition, for stable flows, wall cooling was found to limit either the upstream or the downstream propagation of disturbances and thereby have a dramatic effect on both the location and size of the recirculation zone. Finally, the present numerical results were found to blend smoothly with those in regime 3 predicted by the analytic theory of Kerimbekov *et al.* (1994) for strong wall cooling.

The hypersonic formulation with wall cooling used in the present investigation follows the seminal work of Neiland (1973), wherein the terms 'supercritical', 'transcritical' and 'subcritical' connoted the state of the upstream boundary layer for

$\bar{M} > 1$, $\bar{M} \sim 1$ and $\bar{M} < 1$, respectively. More recently, Brown *et al.* (1990) have considered the problem using a somewhat different approach; they introduced their own terminology in which they used the aforementioned adjectives to delineate the three temperature regimes that have been nominally identified here as 1, 2 and 3, respectively. In the Appendix, a brief comparison of the two approaches is given. In this paper, Neiland's (1973) terminology will be used throughout. The present results for supercritical boundary layers compare very well with those of Brown *et al.* (1990) who sought steady solutions in regime 2, but did not consider the subcritical case. For strong wall cooling, however, the results obtained by Brown *et al.* (1990) do not exhibit the proper behaviour in that the pressure shows continual growth downstream instead of approaching a constant plateau. In contrast, the present results behave as expected and also confirm the scalings of Kerimbekov *et al.* (1994) as regime 2 blends into regime 3. The reasons for the discrepancy with Brown *et al.* (1990) are described in Appendix B of Kerimbekov *et al.* (1994).

2. Hypersonic triple deck with wall cooling

The two-dimensional hypersonic triple-deck formulation for a flat-plate boundary layer with wall cooling was first considered by Neiland (1973) and will be investigated here. Consider a plate of length L which is oriented parallel to the flow of an ideal compressible gas having speed U_∞, density ρ_∞, enthalpy h_∞ and pressure p_∞. The specific heat ratio γ is taken to be constant. A semi-infinite plate is joined to the downstream end of the first plate and inclined at a small angle α' to the flow direction, thereby forming a compression ramp on the upper surface of the composite body. Define flow variables such that lengths, velocities, the pressure, density, enthalpy and absolute viscosity are made dimensionless with respect to L, U_∞, $\rho_\infty U_\infty^2$, ρ_∞, U_∞^2, and μ_0, respectively. Here, μ_0 denotes the viscosity evaluated at a reference enthalpy of U_∞^2. The viscosity is taken to be a function of temperature alone and given by the power law $\mu' = (h')^n$, where n is a positive constant. Here, and throughout, the prime will be used to denote unscaled dimensionless variables. The Reynolds number Re_0 and upstream Mach number M_∞ are defined by

$$Re_0 = \frac{\rho_\infty U_\infty L}{\mu_0}, \qquad M_\infty = U_\infty \left(\frac{\gamma p_\infty}{\rho_\infty}\right)^{-1/2}, \tag{2.1a,b}$$

and both are assumed to be large, but such that the hypersonic viscous interaction parameter χ is small, namely

$$\chi = M_\infty^2 Re_0^{-1/2} \ll 1. \tag{2.2}$$

This condition requires that the corner of the ramp be located in a region of weak global viscous interaction.

As discussed by Neiland (1973) and Kerimbekov *et al.* (1994), the upstream boundary layer bifurcates into two layers when the wall temperature is sufficiently low. The main part of the boundary layer is denoted as region β in figure 1, and the streamwise velocity u' and enthalpy h' in this region are functions of x' and the scaled normal variable $Y = M_\infty^{-1} Re_0^{1/2} y'$. In addition, the density $\rho' = M_\infty^{-2} R(x', Y)$ is small, where the scaled density function R is $O(1)$. The mainstream enthalpy (non-dimensionalized by U_∞^2) is $O(M_\infty^{-2})$ as $M_\infty \to \infty$, and consequently the matching conditions to the mainstream are

$$u' \to 1, \quad h' \to 0 \quad \text{as} \quad Y \to \delta(x'), \tag{2.3a,b}$$

where $\delta(x')$ denotes the upstream boundary-layer thickness. At the plate surface

$$u' = 0, \quad h' = g_w = \frac{h_w^*}{U_\infty^2}, \tag{2.4a,b}$$

where h_w^* denotes the dimensional wall enthalpy. The quantity g_w is called the temperature factor, and the physical situation of interest here is when the wall is cold in the sense that $g_w \ll 1$. In general, the dependent variables in layer β are such that

$$u' \sim Y^{1/(n+1)}, \quad h' \sim Y^{1/(n+1)}, \quad R \sim Y^{-1/(n+1)}, \tag{2.5a–c}$$

as $Y \to 0$ (Kerimbekov *et al.* 1994), and consequently the solution is not uniformly valid. An inner layer (denoted as α^* in figure 1) is required in order to adjust the solution for h' to condition (2.4*b*), as well as the scaled density function R to a finite value on the wall. In region α^*, the solution is a function of x' and the scaled variable $\hat{Y} = M_\infty^{-1} Re_0^{1/2} g_w^{-(n+1)} y' = g_w^{-(n+1)} Y$, while u' and h' are $O(g_w)$ with $\rho' = O(M_\infty^{-2} g_w^{-1})$. As shown by Kerimbekov *et al.* (1994), the solution in region α is such that

$$u' \to g_w \lambda \hat{Y}, \quad h' \to g_w \quad \text{as} \quad \hat{Y} \to 0, \tag{2.6a,b}$$

as the interaction region is approached (i.e. $x' \to 1$). Here, λ is an $O(1)$ constant whose value must be determined from a global solution of the upstream boundary-layer flow.

In the vicinity of the compression ramp (or equivalently some other streamwise disturbance), a multi-layer structure develops as shown in figure 1. Regions I_α and II are simply continuations of the regions α^* and β in the upstream boundary layer, respectively, while region III constitutes a region of inviscid potential flow above the boundary layer. When the ramp angle α' is $O(Re_0^{-1/4})$, a nonlinear response to the changes in pressure provoked by the compression ramp occurs in the sublayer I, while perturbations to the flow in regions I_α, II and III remain linear. The scalings and the nature of the solution in each of these regions have been described by Kerimbekov *et al.* (1994), and the lower-deck problem depends on the following scaled variables:

$$x' - 1 = (\gamma - 1)^{1/2} \lambda^{-5/4} M_\infty^{3/2} g_w^{n+1/2} Re_0^{-3/8} x, \tag{2.7a}$$

$$y' = (\gamma - 1)^{1/2} \lambda^{-3/4} M_\infty^{3/2} g_w^{n+1/2} Re_0^{-5/8} \{y - f(x)\}, \tag{2.7b}$$

$$u' = (\gamma - 1)^{1/2} \lambda^{1/4} M_\infty^{1/2} g_w^{1/2} Re_0^{-1/8} u(x, y, t), \tag{2.7c}$$

$$v' = (\gamma - 1)^{1/2} \lambda^{3/4} M_\infty^{1/2} g_w^{1/2} Re_0^{-3/8} \{v(x, y, t) - \mathrm{d}f/\mathrm{d}x\}, \tag{2.7d}$$

$$p' - 1 = \gamma \lambda^{1/2} M_\infty^{-1} Re_0^{-1/4} p(x, t), \tag{2.7e}$$

$$t' = \lambda^{-3/2} M_\infty g_w^n Re_0^{-1/4} t. \tag{2.7f}$$

Here, the body contour is defined by $y = f(x)$, and a Prandtl transposition has been incorporated in equations (2.7). It can be shown (Kerimbekov *et al.* 1994) that in the lower deck, the density $\rho' = M_\infty^{-2} g_w^{-1} (\gamma - 1)^{-1}$ and the enthalpy $h' = g_w$ are constant, and the remaining dependent variables satisfy the triple-deck problem

$$\frac{\partial u}{\partial t} + u \frac{\partial u}{\partial x} + v \frac{\partial u}{\partial y} = -\frac{\partial p}{\partial x} + \frac{\partial^2 u}{\partial y^2}, \quad \frac{\partial u}{\partial x} + \frac{\partial v}{\partial y} = 0, \tag{2.8a,b}$$

with the interaction law

$$p = -\frac{\partial A}{\partial x} + \frac{\mathrm{d}f}{\mathrm{d}x} + S \mathscr{L} \frac{\partial p}{\partial x}, \tag{2.9}$$

and boundary conditions

$$u = v = 0 \quad \text{at} \quad y = 0, \tag{2.10a}$$

$$u \to y + \ldots \quad \text{as} \quad x \to -\infty, \tag{2.10b}$$

$$u \sim y + A(x,t) + \ldots \quad \text{as} \quad y \to \infty. \tag{2.10c}$$

In equation (2.9), the parameters S and $\mathscr{L}$ are defined by

$$S = (\gamma - 1)^{-1/2}\lambda^{5/4}M_\infty^{1/2}g_w^{-(n+1/2)}Re_0^{-1/8}, \quad \mathscr{L} = \int_0^{\delta_0}\left[\frac{1}{M_0^2} - 1\right]\mathrm{d}Y, \tag{2.11a,b}$$

where δ_0 is the boundary-layer thickness, and $M_0(Y)$ is the Mach number distribution across the boundary layer just upstream of the interaction region. Finally, the ramp angle is given by

$$\alpha' = \lambda^{1/2}Re_0^{-1/4}\alpha. \tag{2.12}$$

If the average upstream Mach number is less than one, $\mathscr{L} > 0$, and this is called the subcritical case. On the other hand, if the average upstream Mach number is greater than one, then $\mathscr{L} < 0$, and this is referred to as the supercritical case. The terminology 'cold wall' is utilized in the present context to imply that the parameter S is $O(1)$ which can occur only when the temperature factor $g_w \ll 1$. Note from equation (2.9) that when $S\mathscr{L} \to 0$, corresponding to moderate to high wall temperatures, the formulation reduces to the classical triple-deck problem for supersonic flows (Stewartson & Williams 1969; Neiland 1969).

Tutty & Cowley (1986) have discussed the possibility of physical instabilities occurring in the unsteady triple-deck formulation, and Cassel *et al.* (1995) have shown that an instability is present in the supersonic triple-deck problem (as well as the hypersonic case) for moderate wall temperatures. This instability was shown to develop within the region of reversed flow that develops near the corner once the ramp angle exceeds a certain critical value. For ramp angles above the critical value, inflection points form in the velocity profiles near the corner and this appears to lead to an absolute instability in the form of a wave packet that ultimately forms near the corner but remains stationary. Following the procedure described by Tutty & Cowley (1986), infinitesimal short-wave disturbances of the form

$$u(x,y,t) = u_0(x,y,t) + \varepsilon \mathrm{e}^{\mathrm{i}(\tilde{\alpha}x - \tilde{\alpha}ct)}u_1(x,y,t) + \ldots, \tag{2.13}$$

are assumed, where $\varepsilon \ll 1, \tilde{\alpha}$ is large and real, and $c = c_r + \mathrm{i}c_i$ is the complex wave speed; if $c_i > 0$, any small disturbance will grow and cause an instability. Using the procedures described by Tutty & Cowley (1986) and Cassel (1993), it is readily shown that a necessary and sufficient condition for instability is

$$\int_0^\infty \frac{\mathrm{d}y}{(u_0 - c)^2} = -S\mathscr{L}. \tag{2.14}$$

For a known base velocity profile u_0, this provides an eigenvalue relation for the complex wave speed for a given level of wall cooling S and a given type of upstream velocity profile characterized by $\mathscr{L}$. As discussed by Tutty & Cowley (1986) and Cassel *et al.* (1995), when $S = 0$, corresponding to either the supersonic or hypersonic triple deck without wall cooling, Rayleigh's and Fjørtoft's theorems are necessary conditions for a high-wavenumber instability. However, when $S\mathscr{L} \neq 0$, it is only possible to show from equation (2.14) that an instability can occur if $\partial^2 u_0/\partial y^2 > 0$ for

at least part of the interval $0 < y < \infty$; this condition replaces Rayleigh's theorem in the cold wall case but is not considered to be especially useful since it lacks specificity. In addition, it does not appear that there is a condition for the cold wall case which is analogous to Fjørtoft's theorem.

3. Strong wall cooling singularities

As described by Kerimbekov *et al.* (1994), the three temperature regimes depend on the magnitude of the wall temperature factor g_w, and hence S, or equivalently the Neiland number defined by

$$N = (S\,|\mathscr{L}|)^{4/3}. \tag{3.1}$$

The three regimes are defined by: (1) $N \ll 1$ or $g_w \gg \chi^{1/(4n+2)}$; (2) $N = O(1)$ or $g_w \sim \chi^{1/(4n+2)}$ and (3) $N \gg 1$ or $g_w \ll \chi^{1/(4n+2)}$. Kerimbekov *et al.* (1994) considered the third regime wherein the wall is cooled so strongly that the displacement effect due to the main deck dominates that of the viscous sublayer, which ultimately becomes too small to influence the leading-order external pressure distribution (Neiland & Socolov 1975). Such interactions are therefore inviscid–inviscid between the main deck and the outer flow. The Neiland number N represents the ratio of the contributions to the displacement thickness due to the main deck and the viscous sublayer. For $N \to \infty$, a rescaling of variables in the system is necessary according to

$$x = N^{3/4}\bar{x}, \quad y = N^{1/4}\bar{y}, \tag{3.2a,b}$$

$$u = N^{1/4}\bar{u}(\bar{x},\bar{y}), \quad v = N^{-1/4}\bar{v}(\bar{x},\bar{y}), \quad p = N^{1/2}\bar{p}(\bar{x}), \tag{3.2c–e}$$

$$A = N^{1/4}\bar{A}(\bar{x}), \quad f = N^{5/4}\bar{f}(\bar{x}). \tag{3.2f,g}$$

Defining a streamfunction by $\bar{u} = \partial\bar{\psi}/\partial\bar{y}$, $\bar{v} = -\partial\bar{\psi}/\partial\bar{x}$, the formulation in equations (2.8)–(2.10) for steady flow becomes

$$\frac{\partial\bar{\psi}}{\partial\bar{y}}\frac{\partial^2\bar{\psi}}{\partial\bar{x}\partial\bar{y}} - \frac{\partial\bar{\psi}}{\partial\bar{x}}\frac{\partial^2\bar{\psi}}{\partial\bar{y}^2} = -\frac{\partial\bar{p}}{\partial\bar{x}} + \frac{\partial^3\bar{\psi}}{\partial\bar{y}^3}, \tag{3.3}$$

with the interaction law

$$\bar{p} = -\frac{1}{N}\frac{\partial\bar{A}}{\partial\bar{x}} + \frac{\partial\bar{f}}{\partial\bar{x}} + \mathrm{sgn}(\mathscr{L})\frac{\partial\bar{p}}{\partial\bar{x}}, \tag{3.4}$$

and boundary conditions

$$\bar{\psi} = \frac{\partial\bar{\psi}}{\partial\bar{y}} = 0 \quad \text{at} \quad \bar{y} = 0, \tag{3.5a}$$

$$\bar{\psi} \sim \tfrac{1}{2}\bar{y}^2 + A(\bar{x})\bar{y} + \ldots \quad \text{as} \quad \bar{y} \to \infty, \text{ and as } \bar{x} \to -\infty. \tag{3.5b}$$

The surface geometry of the compression ramp is given by

$$\bar{f}(\bar{x}) = \begin{cases} 0, & \bar{x} < 0 \\ \\ \bar{\alpha}\bar{x}, & \bar{x} > 0 \end{cases}, \tag{3.6}$$

where the ramp angle (cf. equation (2.12)) is defined by $\bar{\alpha} = N^{-1/2}\alpha$ and $\bar{\alpha}$ is assumed to be $O(1)$. Note that in these variables the interaction problem depends only on the magnitude of N and the sign of $\mathscr{L}$. It is evident from equation (3.4) that as N becomes large, the first term in the interaction law, representing the contribution to the displacement thickness due to the viscous sublayer, becomes small.

Kerimbekov *et al.* (1994) considered solutions of the system (3.3)–(3.6) for both the subcritical ($\mathscr{L} > 0$) and supercritical ($\mathscr{L} < 0$) wall cooling cases. The form of the interaction law (3.4) suggests the following expansions for the streamfunction, pressure distribution and displacement function:

$$\bar{\psi}(\bar{x}, \bar{y}) = \psi_o(\bar{x}, \bar{y}) + N^{-1}\psi_1(\bar{x}, \bar{y}) + ..., \tag{3.7a}$$

$$\bar{p}(\bar{x}) = p_o(\bar{x}) + N^{-1}p_1(\bar{x}) + ..., \quad \bar{A}(\bar{x}) = A_o(\bar{x}) + N^{-1}A_1(\bar{x}) + ..., \tag{3.7b,c}$$

and substitution into the interaction law (3.4) gives the following equation for the leading-order pressure term:

$$p_0 = \mathrm{sgn}(\mathscr{L})\frac{\partial p_0}{\partial \bar{x}} + \bar{\alpha}H(\bar{x}), \tag{3.8}$$

where $H(\bar{x})$ is the Heaviside function. For a supercritical boundary layer ($\mathscr{L} < 0$), the solution of equation (3.8) is

$$p_0 = \begin{cases} 0, & \bar{x} < 0 \\ \bar{\alpha}(1 - \mathrm{e}^{-\bar{x}}), & \bar{x} > 0 \end{cases}, \tag{3.9}$$

while for a subcritical boundary layer ($\mathscr{L} > 0$),

$$p_0 = \begin{cases} \bar{\alpha}\mathrm{e}^{\bar{x}}, & \bar{x} < 0 \\ \bar{\alpha}, & \bar{x} > 0. \end{cases} \tag{3.10}$$

Consequently, for the supercritical case (3.9), there are no disturbances upstream of $\bar{x} = 0$, and the pressure starts to increase only at the corner toward $\bar{\alpha}$ as $\bar{x} \to \infty$. On the other hand, for the subcritical case (3.10), the pressure increases from zero far upstream to $\bar{\alpha}$ at the corner and is then constant along the ramp itself. Substituting equations (3.7*a*, *b*) into the momentum equation (3.3) in the viscous sublayer gives

$$\frac{\partial \psi_0}{\partial \bar{y}}\frac{\partial^2 \psi_0}{\partial \bar{x}\partial \bar{y}} - \frac{\partial \psi_0}{\partial \bar{x}}\frac{\partial^2 \psi_0}{\partial \bar{y}^2} = -\frac{\partial p_0}{\partial \bar{x}} + \frac{\partial^3 \psi_0}{\partial \bar{y}^3}, \tag{3.11}$$

and the boundary conditions are

$$\psi_0 = \frac{\partial \psi_0}{\partial \bar{y}} = 0 \quad \text{at} \quad \bar{y} = 0, \tag{3.12a}$$

$$\psi_0 \sim \tfrac{1}{2}\bar{y}^2 + A_0(\bar{x})\bar{y} + ... \quad \text{as} \quad \bar{y} \to \infty, \quad \text{and as } \bar{x} \to -\infty. \tag{3.12b}$$

Since the problem (3.11),(3.12) is a classical boundary-layer problem with prescribed pressure gradient given by either of equations (3.9) or (3.10), the solutions may be obtained using a conventional numerical procedure starting from the initial condition $\partial \psi_0/\partial \bar{y} \to \bar{y}$ as $\bar{x} \to -\infty$ and marching in the positive $\bar{x}$-direction. Such solutions were obtained by Kerimbekov *et al.* (1994) for the supercritical pressure distribution (3.9) and were found to exhibit the phenomenon of marginal separation for increasing ramp angle $\bar{\alpha}$. For each $\bar{\alpha}$, there is a minimum in wall shear, which decreases with increasing ramp angle until eventually a zero is reached at a critical ramp angle $\bar{\alpha}_0 = 0.7548$ at $\bar{x} = \bar{x}_0 = 0.5$. This type of behaviour also occurs in the boundary layer near the leading edge of thin airfoils at some critical angle of attack. The marginal separation theory of Stewartson *et al.* (1982) and Ruban (1981) for the airfoil problem shows that a singularity develops at the point of zero wall shear at $\bar{x}_0$ as the critical angle is approached. However, the singularity is weak in the sense that solutions of the boundary-layer equations may be continued downstream of $\bar{x}_0$. A local interaction

region forms near $\bar{x}_0$ in order to relieve the singularity (Stewartson *et al.* 1982; Ruban 1982). Kerimbekov *et al.* (1994) show that marginal separation theory applies to the supercritical wall cooling case for large Neiland number. Numerical solutions for large, but finite, values of N will be described in §6 and compared with the analytical results for $N \to \infty$.

For the subcritical wall cooling case, the solution of equation (3.11) subject to the prescribed pressure distribution (3.10) exhibits a Goldstein (1948) singularity at a point of zero wall shear on the flat surface upstream of the corner, for a sufficiently high ramp angle $\bar{\alpha}$. However, the singularity can be removed by a series of regions which have successively shorter streamwise length scales allowing for a smooth transition into a separated region downstream (Smith & Daniels 1981). Physically, this type of situation is sometimes described as a compensation regime in which the combination of the surface shape and the displacement thickness of the boundary layer cancel such that the streamlines at the outer edge of the boundary layer are horizontal.

4. Formulation

In the present investigation, wall temperatures in regime 2, for which $N = O(1)$, are of interest, and the problem considered is governed by equations (2.8)–(2.10). As described by Cassel *et al.* (1995), an equation for the shear stress $\tau = \partial u/\partial y$ may be obtained by differentiating equation (2.8*a*) with respect to y. In addition, a streamfunction is defined by $u = \partial\psi/\partial y$, $v = -\partial\psi/\partial x$ and is related to τ by $\partial^2\psi/\partial y^2 = \tau$. The displacement function $A(x,t)$ in equation (2.10*c*) is given by

$$A(x,t) = \lim_{y\to\infty}(u - y) = \lim_{y\to\infty}\int_0^y (\tau - 1)\mathrm{d}y, \tag{4.1}$$

and by differentiation of the interaction law using the procedures discussed by Cassel *et al.* (1995), it is easily shown that

$$\left.\frac{\partial\tau}{\partial y}\right|_{y=0} = -\frac{\partial^2}{\partial x^2}\int_0^\infty (\tau - 1)\mathrm{d}y + \frac{\mathrm{d}^2 f}{\mathrm{d}x^2} + S\mathscr{L}\frac{\partial}{\partial x}\left[\left.\frac{\partial\tau}{\partial y}\right|_{y=0}\right]. \tag{4.2}$$

In this manner the interaction is expressed in terms of the wall shear. Note that an equation for the wall shear stress has also been used extensively by Burggraf & Duck (1982) and Duck (1987).

It is convenient to transform the infinite flow domain into a finite rectangular domain using the transformations

$$\hat{x} = \frac{2}{\pi}\arctan\left(\frac{x}{a}\right), \quad \hat{y} = \frac{2}{\pi}\arctan\left(\frac{y}{b}\right). \tag{4.3a,b}$$

Here the parameters a and b determine the level of grid packing in physical space with smaller values of a and b implying a greater concentration of grid points near the ramp corner at $x = 0$ and the surface at $y = 0$, respectively. It is easily shown that the interaction problem in these variables is

$$\frac{\partial\tau}{\partial t} + \frac{\Gamma(\hat{x})}{a}u\frac{\partial\tau}{\partial\hat{x}} + \frac{\Gamma(\hat{y})}{b}v\frac{\partial\tau}{\partial\hat{y}} = \frac{\Gamma(\hat{y})}{b}\frac{\Gamma'(\hat{y})}{b}\frac{\partial\tau}{\partial\hat{y}} + \frac{\Gamma^2(\hat{y})}{b^2}\frac{\partial^2\tau}{\partial\hat{y}^2}, \tag{4.4}$$

for τ, where $\Gamma(\zeta) = [1 + \cos(\pi\zeta)]/\pi$. The boundary conditions (2.10*b*,*c*) reduce to

$$\tau \to 1 \quad \text{as} \quad \hat{x} \to \pm 1, \quad \tau \to 1 \quad \text{as} \quad \hat{y} \to 1, \tag{4.5a,b}$$

and the interaction law (4.2) becomes

$$\frac{\Gamma(0)}{b}\left.\frac{\partial\tau}{\partial\hat{y}}\right|_{\hat{y}=0} = -\left[\frac{\Gamma(\hat{x})}{a}\frac{\Gamma'(\hat{x})}{a}\frac{\partial}{\partial\hat{x}} + \frac{\Gamma^2(\hat{x})}{a^2}\frac{\partial^2}{\partial\hat{x}^2}\right] b\int_0^1 \frac{\tau-1}{\Gamma(\hat{y})}\mathrm{d}\hat{y} + \frac{\mathrm{d}^2 f}{\mathrm{d}x^2} + S\mathscr{L}\frac{\Gamma(\hat{x})}{a}\frac{\partial}{\partial\hat{x}}\left[\frac{\Gamma(0)}{b}\left.\frac{\partial\tau}{\partial\hat{y}}\right|_{\hat{y}=0}\right]. \tag{4.6}$$

The equations relating the streamfunction and shear stress are

$$\frac{\Gamma(\hat{y})}{b}\frac{\partial}{\partial\hat{y}}\left[\frac{\Gamma(\hat{y})}{b}\frac{\partial\psi}{\partial\hat{y}}\right] = \tau, \quad \psi|_{\hat{y}=0} = \left.\frac{\partial\psi}{\partial\hat{y}}\right|_{\hat{y}=0} = 0. \tag{4.7a,b}$$

The velocity components are obtained from

$$u = \frac{\Gamma(\hat{y})}{b}\frac{\partial\psi}{\partial\hat{y}}, \quad v = -\frac{\Gamma(\hat{x})}{a}\frac{\partial\psi}{\partial\hat{x}}. \tag{4.8a,b}$$

5. Numerical methods

The algorithm described by Cassel *et al.* (1995) was extended here to include the effects of wall cooling, and only a brief summary of the approach is given here. Steady-state solutions for each value of $S\mathscr{L}$ and the scaled ramp angle α were sought as the large-time limit of an unsteady integration initiated from the flat-plate solution $\tau = 1$ at $t = 0$. A solution to the momentum equation (4.4) and the interaction law (4.6) is required at each time step; the streamfunction and u were then obtained from integration of equation (4.7*a*) with v being evaluated from equation (4.8*b*). Let y_{max} denote the finite value of y at which the vertical extent of the domain was truncated. The $\hat{x}$ interval was divided into a uniform mesh having $I-1$ subintervals of length $\Delta\hat{x}$, and the $\hat{y}$ interval from zero to $\hat{y}_{max}$ was divided into a uniform mesh having $J-1$ subintervals of length $\Delta\hat{y}$. The dependent variables evaluated at the point $(\hat{x}_i, \hat{y}_j)$ at the current time step (where the solution is sought) are denoted by subscripts i and j. In the numerical approximations to equation (4.4) described by Cassel *et al.* (1995), the time derivative is approximated by a simple backward difference, while $\partial\tau/\partial\hat{y}$ and $\partial^2\tau/\partial\hat{y}^2$ are represented by conventional central differences; $u\partial\tau/\partial\hat{x}$ and v are approximated at the previous time step, where the solution is known, and $\partial\tau/\partial\hat{x}$ is represented by a second-order upwind-downwind formula that is dependent on the sign of u. Thus the method is second-order accurate in space but first-order accurate in time. These approximations lead to a formula for $\tau_{i,j}$ at each time step of the form

$$\tau_{i,j} = C_{i,j}\tau_{i,1} + B_{i,j}, \quad j = 2, ..., J, \tag{5.1}$$

where the arrays $C_{i,j}$ and $B_{i,j}$ are evaluated using recursion relations given by Cassel *et al.* (1995). Consequently, the shear stress $\tau_{i,j}$ may be determined at time t once the wall shear is known.

To obtain the shear stress on the wall, discretization of the interaction law (4.6) gives a tridiagonal system for the wall shear stress, in a manner similar to that described by Cassel *et al.* (1995), which is of the form

$$\bar{c}_i^{-}\tau_{i-1,1} + \bar{c}_i\tau_{i,1} + \bar{c}_i^{+}\tau_{i+1,1} = \bar{d}_i, \quad i = 2, ..., I-1, \tag{5.2}$$

where

$$\bar{c}_i = \frac{\Gamma^2(\hat{x}_i)}{a^2}\frac{2N_i}{(\Delta\hat{x})^2} - \left[\frac{\Gamma(0)}{b}\frac{4C_{i,2}-3-C_{i,3}}{2\Delta\hat{y}}\right], \tag{5.3a}$$

$$\bar{c}_i^- = -\frac{\Gamma^2(\hat{x}_i)}{a^2}\frac{N_{i-1}}{(\Delta\hat{x})^2} + \frac{\Gamma(\hat{x}_i)}{a}\frac{\Gamma'(\hat{x}_i)}{a}\frac{N_{i-1}}{2\Delta\hat{x}} - S\mathscr{L}\frac{\Gamma(\hat{x}_i)}{a}\frac{\Gamma(0)}{b}\frac{1}{2\Delta\hat{x}}\left[\frac{4C_{i-1,2} - 3 - C_{i-1,3}}{2\Delta\hat{y}}\right], \tag{5.3b}$$

$$\bar{c}_i^+ = -\frac{\Gamma^2(\hat{x}_i)}{a^2}\frac{N_{i+1}}{(\Delta\hat{x})^2} - \frac{\Gamma(\hat{x}_i)}{a}\frac{\Gamma'(\hat{x}_i)}{a}\frac{N_{i+1}}{2\Delta\hat{x}} + S\mathscr{L}\frac{\Gamma(\hat{x}_i)}{a}\frac{\Gamma(0)}{b}\frac{1}{2\Delta\hat{x}}\left[\frac{4C_{i+1,2} - 3 - C_{i+1,3}}{2\Delta\hat{y}}\right], \tag{5.3c}$$

$$\begin{aligned}\bar{d}_i = {} & \frac{\Gamma^2(\hat{x}_i)}{a^2}\left[\frac{M_{i+1} - 2M_i + M_{i-1}}{(\Delta\hat{x})^2}\right] \\ & + \frac{\Gamma(\hat{x}_i)}{a}\frac{\Gamma'(\hat{x}_i)}{a}\left[\frac{M_{i+1} - M_{i-1}}{2\Delta\hat{x}}\right] \\ & - \left.\frac{\mathrm{d}^2 f}{\mathrm{d}x^2}\right|_{x=x_i} + \frac{\Gamma(0)}{b}\left[\frac{4B_{i,2} - B_{i,3}}{2\Delta\hat{y}}\right] \\ & - S\mathscr{L}\frac{\Gamma(\hat{x}_i)}{a}\frac{\Gamma(0)}{b}\frac{1}{2\Delta\hat{x}}\left[\frac{4B_{i+1,2} - B_{i+1,3}}{2\Delta\hat{y}} - \frac{4B_{i-1,2} - B_{i-1,3}}{2\Delta\hat{y}}\right].\end{aligned} \tag{5.3d}$$

The coefficients M_i and N_i are defined in terms of the arrays C_{ij} and B_{ij} in equations (4.13) of Cassel *et al.* (1995). The tridiagonal system (5.2), (5.3) was solved for the wall shear $\tau_{i,1}$ using the Thomas algorithm subject to the boundary conditions $\tau_{1,1} = \tau_{I,1} = 1$, and the shear stress throughout the two-dimensional domain was then computed from equation (5.1) for $i = 2, ..., I-1$. The streamfunction ψ and u were then obtained by integration of equation (4.7*a*) using the trapezoidal rule, and v was calculated using a central difference approximation to equation (4.8*b*).

The pressure distribution may also be computed at any desired time from the wall shear stress distribution. The pressure equation is obtained from substitution of equations (4.1) and (4.2) into the original interaction law (2.9) giving

$$p = -\frac{\Gamma(\hat{x})}{a}\frac{\partial}{\partial\hat{x}}\left[b\int_0^{\hat{y}_{max}}\frac{\tau - 1}{\Gamma(\hat{y})}\mathrm{d}\hat{y}\right] + \frac{\mathrm{d}f}{\mathrm{d}x} + S\mathscr{L}\frac{\Gamma(\hat{x})}{a}\frac{\partial p}{\partial\hat{x}}. \tag{5.4}$$

Using second-order central difference approximations for the $\hat{x}$-derivatives and approximating the integral in equation (5.4) as described by Cassel *et al.* (1995) yields a tridiagonal system for the pressure distribution of the form

$$\tilde{c}_i^- p_{i-1} + \tilde{c}_i p_i + \tilde{c}_i^+ p_{i+1} = \tilde{d}_i, \qquad i = 2, ..., I-1, \tag{5.5}$$

where the coefficients are

$$\tilde{c}_i = -1, \quad \tilde{c}_i^- = -S\mathscr{L}\frac{\Gamma(\hat{x}_i)}{a}\frac{1}{2\Delta\hat{x}} = -\tilde{c}_i^+, \tag{5.6a,b}$$

$$\tilde{d}_i = -\frac{\mathrm{d}f}{\mathrm{d}x} + \frac{\Gamma(\hat{x}_i)}{a}\left[\frac{N_{i+1}\tau_{i+1,1} + M_{i+1} - N_{i-1}\tau_{i-1,1} - M_{i-1}}{2\Delta\hat{x}}\right], \tag{5.6c}$$

and the coefficients M_i and N_i are as defined by Cassel *et al.* (1995). For a general

surface shape $f(x)$, the boundary conditions are

$$p_1 = \left.\frac{\mathrm{d}f}{\mathrm{d}x}\right|_{x\to-\infty}, \quad p_I = \left.\frac{\mathrm{d}f}{\mathrm{d}x}\right|_{x\to+\infty}, \tag{5.7}$$

and in particular for the compression ramp $p_1 = 0$, $p_I = \alpha$, where α is the scaled ramp angle.

As described by Cassel *et al.* (1995), a von Neumann stability analysis shows that in order for the numerical solution to remain stable, the time step must be such that

$$\Delta t \leqslant \frac{\pi a \Delta \hat{x}}{4\,|u_{max}|}. \tag{5.8}$$

From the condition (2.10*c*) at the outer edge of the viscous sublayer, the maximum streamwise velocity u_{max} is approximately equal to the normal coordinate y_{max} at which the domain is truncated, and therefore the stability condition (5.8) significantly limits the values of the time step which may be used in order to avoid numerical instability. In practice, the time step was selected to be 50% or less than the restriction implied by equation (5.8)

6. Calculated results

In this section detailed numerical solutions of the hypersonic triple deck with wall cooling will be described for the compression ramp geometry, which was defined by

$$f(x) = \tfrac{1}{2}\alpha\left[x + (x^2 + r^2)^{1/2}\right], \tag{6.1}$$

in order to keep the surface shape smooth. Here, α is the scaled downstream ramp angle and r is the rounding parameter. Calculations were carried out for a range of values of r, but all results shown here are for $r = 0.5$; this value was found to eliminate the difficulties at the corner which result for the true compression ramp ($r = 0$) while minimizing the effect on the overall results. As in Cassel *et al.* (1995), the vertical extent of the computational domain was chosen to be $y_{max} = 50$, which was determined to be sufficiently large to ensure that there is no significant influence on the calculated solutions.

Steady-state solutions were obtained as the large time limit of unsteady calculations for various ramp angles and levels of wall cooling. The initial condition corresponds to a flat plate ($\alpha = 0$) with $u = y$; then at $t = 0$, the ramp angle α was impulsively adjusted to its final value. The unsteady numerical calculation was terminated at some large time when $\partial\tau/\partial t$ was less than 5×10^{-4} at each mesh point along the wall (where the shear stress undergoes the most change).

The effects of wall cooling on the separation and stability characteristics observed by Cassel *et al.* (1995) are of particular interest. Here, the term moderately cooled wall means that the wall temperature factor g_w is small, but that the parameter S, defined in equation (2.11*a*), is $O(1)$. As g_w increases, $S \to 0$, and the moderate wall temperature regime 1 is reached. On the other hand, for very small values of g_w, $S \to \infty$, defining the strong wall cooling case considered by Kerimbekov *et al.* (1994). In addition to the magnitude of S, the hypersonic problem is characterized by the sign of the integral $\mathscr{L}$ in equation (2.11*b*). For hypersonic flows, the supercritical case is expected to be more common when the velocity distribution approaching the corner is described by the flat-plate Blasius solution. Indeed, it can be shown, for example, that when viscosity depends linearly on temperature ($n = 1$) and for Prandtl number $Pr = 1$, the boundary layer on a flat plate is supercritical for cases having

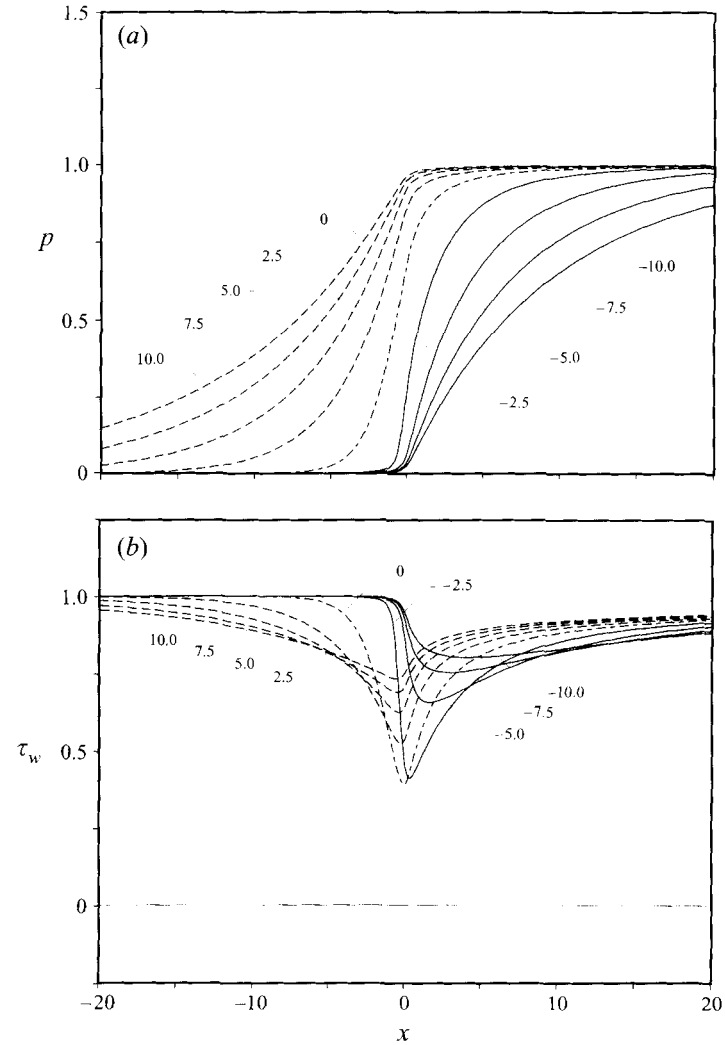

FIGURE 2. Numerical solutions for $\alpha = 1.0$ with various levels of wall cooling; $S\mathscr{L} = -10.0, ..., 10.0$ in increments of 2.5: no cooling effect (– – –), subcritical boundary layer (- - - -), and supercritical boundary layer (—). (*a*) Pressure p, (*b*) wall shear stress τ_w.

specific heat ratio $\gamma < 2.26$ and subcritical for $\gamma > 2.26$ (C. N. Zhikharev 1993, private communication). However, it should be emphasized that the present theory is not restricted to situations where the approach flow is Blasius and more general upstream conditions can give rise to a subcritical boundary layer in air ($\gamma = 1.4$). An interesting possibility arises when the approach flow has $\mathscr{L} = 0$, for which the effects of wall cooling are negated (even for $S = O(1)$); this case has been referred to as transcritical by Neiland (1987).

In the present study, situations where $S\mathscr{L} = O(1)$ are of interest, and results were obtained for both subcritical and supercritical cases. A series of mesh sizes were used for each case as a check on the accuracy. Unless stated otherwise, all results shown were obtained on a mesh defined by $I = 201$, $J = 101$, and $a = b = 10.0$ except for cases with $\alpha = 1.0$, where the mesh was defined by $I = 101$, $J = 51$ and $a = b = 5.0$. A comprehensive set of numerical results with various levels of wall cooling and for

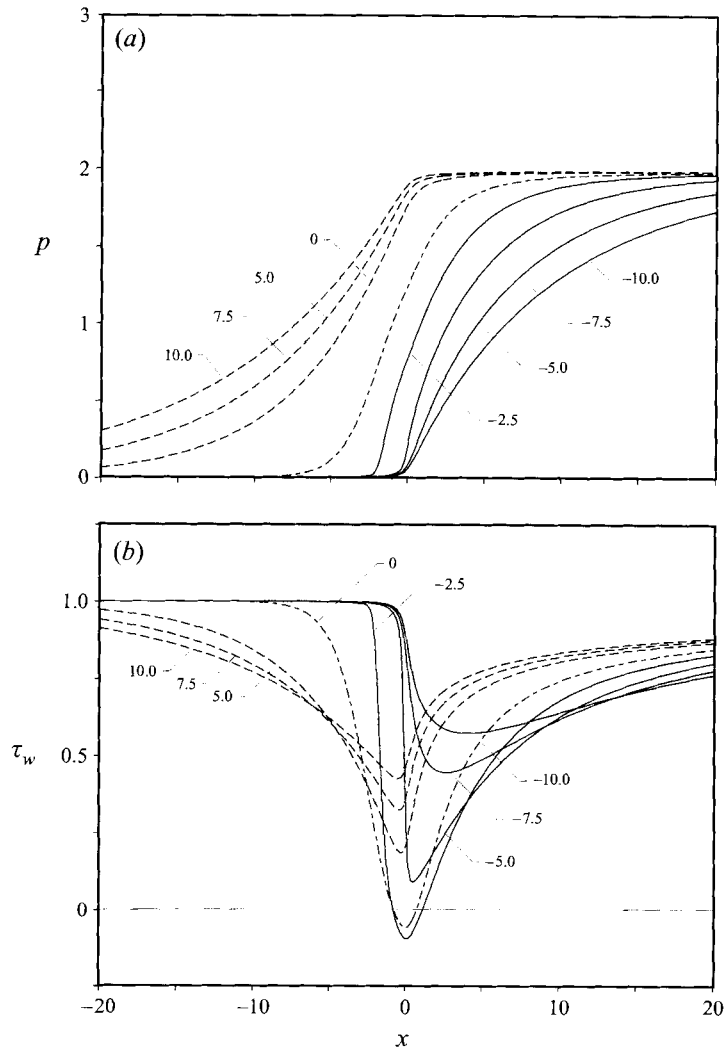

FIGURE 3. As figure 2 but for $\alpha = 2.0$ (cases not shown were unstable).

a series of ramp angles is shown in figures 2–10. Figures 2–6 show pressure and wall shear distributions for a range of both subcritical and supercritical $S\mathscr{L}$ for $\alpha = 1.0$, 2.0, 3.0, 4.0 and 5.0, respectively. Note that for $\alpha \geqslant 2.0$, some cases have been omitted; these are cases for which the solutions became unstable in the form of a wave packet that developed near the corner as described by Cassel *et al.* (1995). Streamlines are shown for ramp angles $\alpha = 3.0$ and 5.0 in figures 7 and 8, respectively, for a series of wall cooling cases in the supercritical regime involving separation. In addition, streamlines for a particular case with $\alpha = 4.0$ and $S\mathscr{L} = -12.5$ are shown in figure 9. The separation and stability characteristics of all the solutions represented in the above-mentioned figures are summarized in figure 10.

One obvious effect of wall cooling which is exhibited in the pressure and wall shear distributions for all ramp angles shown (see figures 2–6) is an inhibition of either upstream or downstream influence as the wall is cooled. For subcritical boundary layers, increased wall cooling reduces the region of influence downstream of the

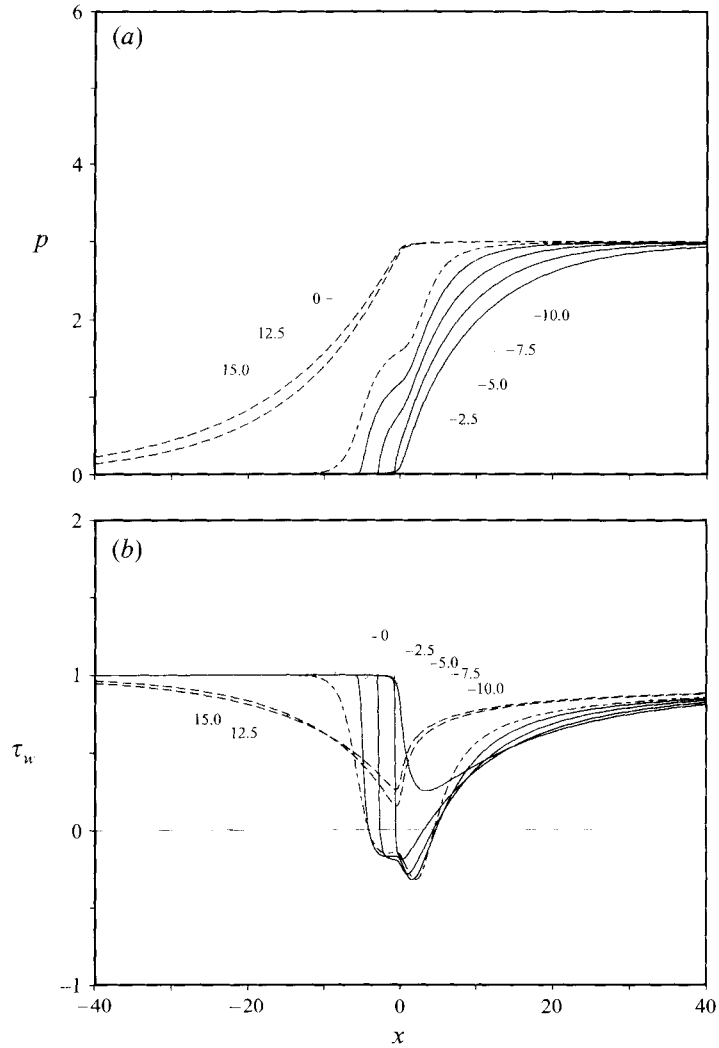

FIGURE 4. As figure 2 but for $\alpha = 3.0$; $S\mathscr{L} = -10.0, ..., 15.0$ in increments of 2.5 (cases not shown were unstable).

compression ramp. This may be observed as a progressive decrease (as the wall is cooled) in the distance downstream of the corner where the pressure achieves its downstream asymptotic value; similarly, the wall shear tends more rapidly to its downstream value as the wall is cooled. For supercritical boundary layers, the opposite behaviour is observed. As the wall is cooled, the upstream influence of the ramp is reduced dramatically, and the point at which the pressure and wall shear begin to rise and fall, respectively, from their upstream values moves downstream into the corner. This reduction in upstream influence as the wall is cooled in the supercritical case has been observed experimentally by Lewis, Kubota & Lees (1968). In the extreme case of very large $S|\mathscr{L}|$, Kerimbekov *et al.* (1994) show that there are no disturbances upstream of the corner in the supercritical case and none downstream of the corner for subcritical flow. In cases where no separation occurs (see figures 2*b* and 3*b*), the wall shear reveals an additional feature. For subcritical boundary layers,

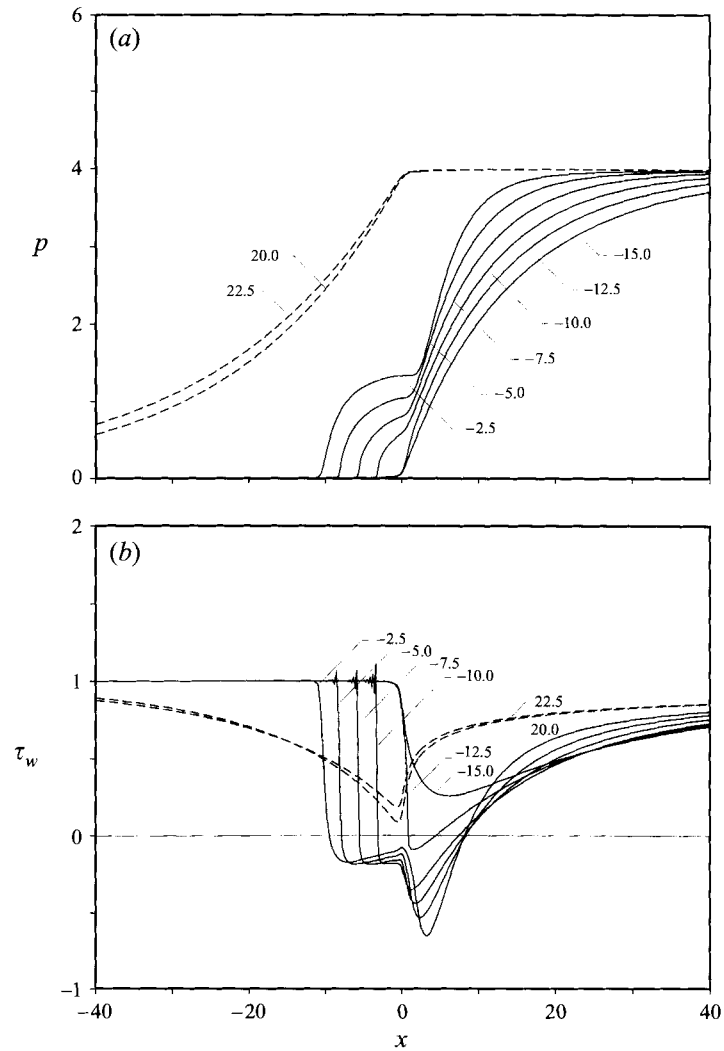

FIGURE 5. As figure 2 but for $\alpha = 4.0$; $S\mathscr{L} = -15.0, \ldots, 22.5$ in increments of 2.5 (cases not shown were unstable).

increases in wall cooling increase the magnitude of the minimum wall shear and shift its streamwise location slightly upstream. An increase in the magnitude of the wall shear minimum also occurs as the wall is cooled for supercritical boundary layers, but in this case the minimum is shifted downstream instead.

Wall cooling has an even more pronounced effect on cases involving separation. It may be noted that for every subcritical case considered where separation occurred, the solution became unstable in the form of a wave packet which remained stationary near the corner as described in Cassel *et al.* (1995). This is reflected in figures 3(*b*), 4(*b*), 5(*b*) and 6(*b*), where τ_w is positive for all x in every case involving subcritical flow in which a stable steady solution was obtained. In contrast, many supercritical cases involving separation remained stable, but wall cooling had a significant effect upon the flow nevertheless. As indicated by the wall shear distribution (figures 3*b*, 4*b*, 5*b* and 6*b*), separation persists for even relatively high values of wall cooling. An additional

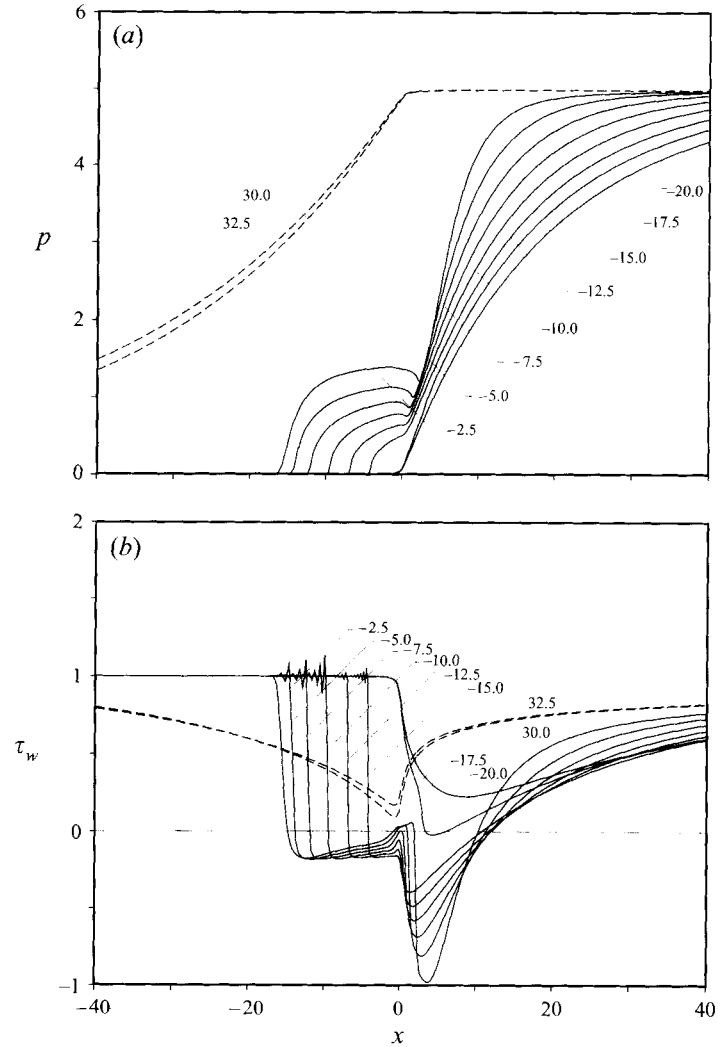

FIGURE 6. As figure 2 but for $\alpha = 5.0$; $S\mathscr{L} = -20.0, ..., 32.5$ in increments of 2.5 (cases not shown were unstable).

feature is that an abrupt drop in wall shear occurs from the upstream value to zero at separation; this drop steepens, moves downstream and occurs over a much shorter streamwise distance as the wall cooling is progressively increased. This sharp, and almost discontinuous, behaviour in wall shear was predicted in the strong wall cooling theory of Kerimbekov *et al.* (1994) and is believed to be the cause of the oscillations observed in the numerical solutions immediately upstream of the separation point for large ramp angles (see figures 5*b* and 6*b*). This behaviour is not believed to be due to an instability because of the streamwise locations where it occurs (well upstream of the corner) and the fact that the amplitudes of the oscillations do not grow with time. Rather, the oscillations are believed to be a numerical consequence of the apparent development of a jump discontinuity in the slope of the wall shear distribution at the upstream limit of influence of the compressive disturbance. Reductions in the spatial mesh resulted in smaller-scale oscillations of comparable magnitude.

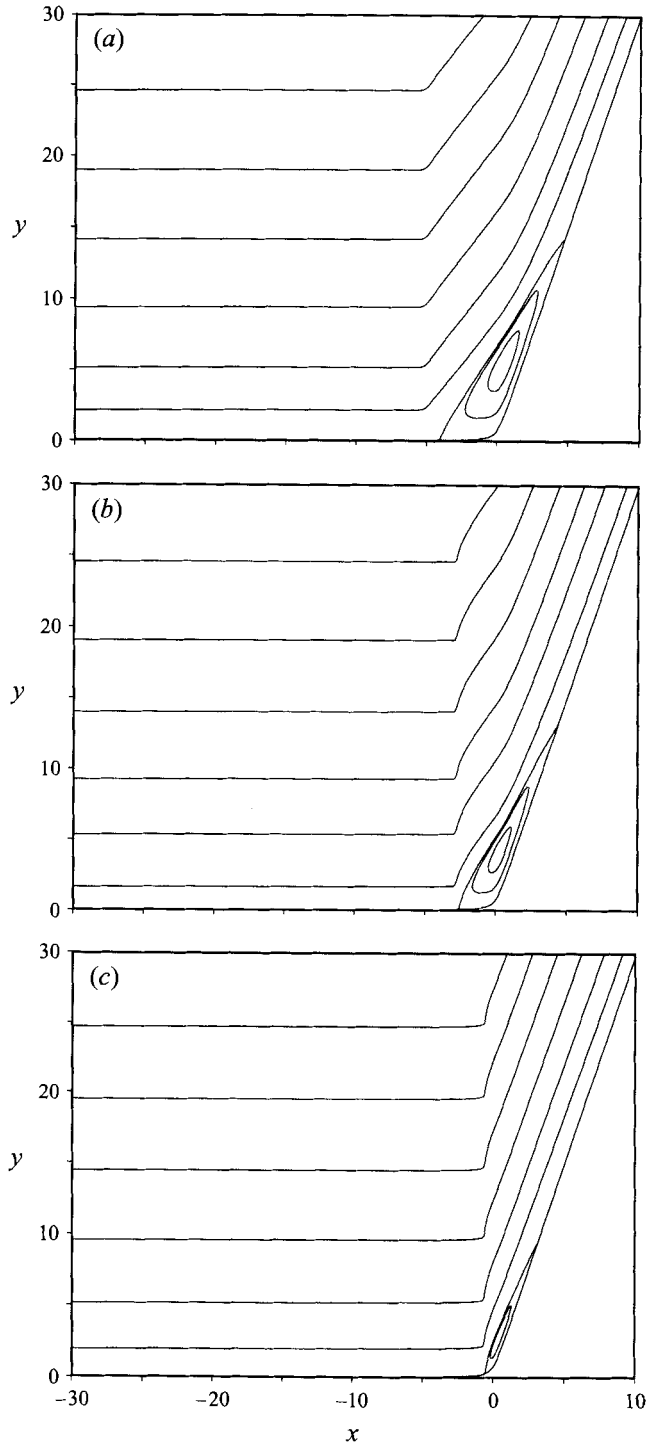

FIGURE 7. Streamlines for $\alpha = 3.0$ as the wall is progressively cooled for supercritical flow. (*a*) $S\mathscr{L} = -2.5$, (*b*) $S\mathscr{L} = -5.0$, (*c*) $S\mathscr{L} = -7.5$.

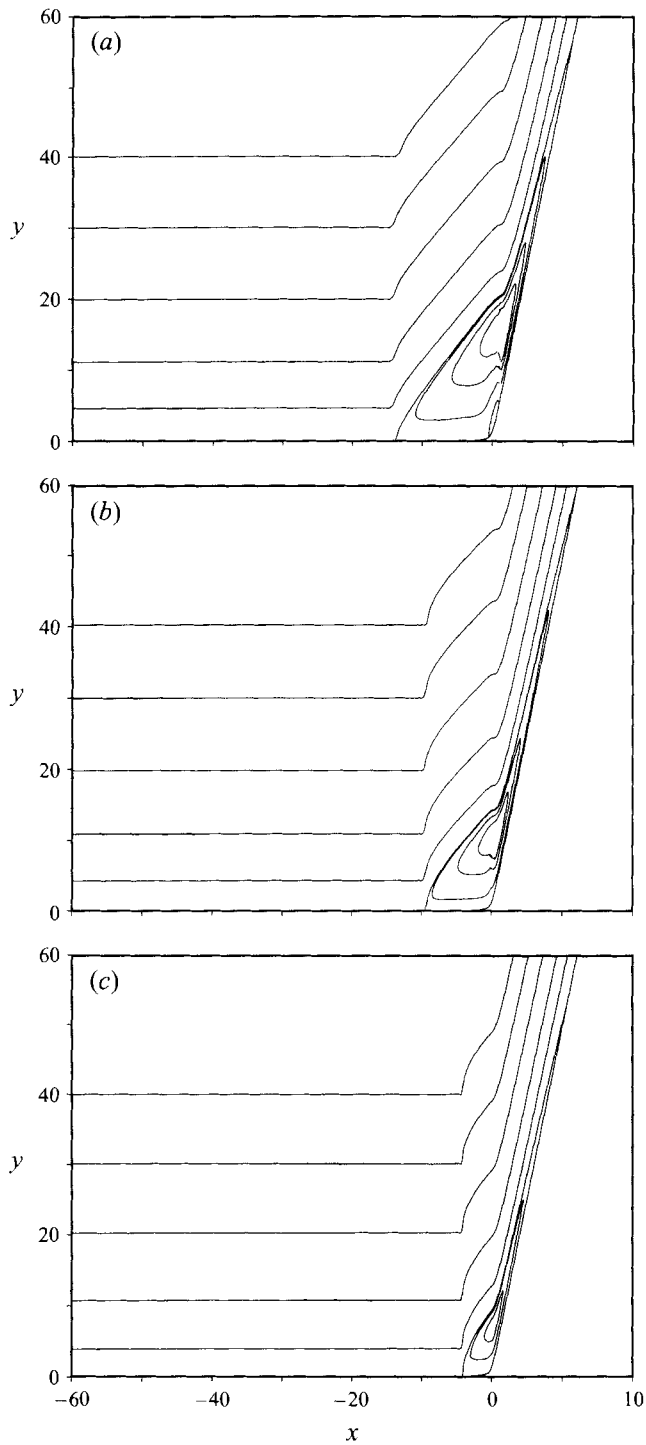

FIGURE 8. Streamlines for $\alpha = 5.0$ as the wall is progressively cooled for supercritical flow. (*a*) $S\mathscr{L} = -5.0$, (*b*) $S\mathscr{L} = -10.0$, (*c*) $S\mathscr{L} = -15.0$.

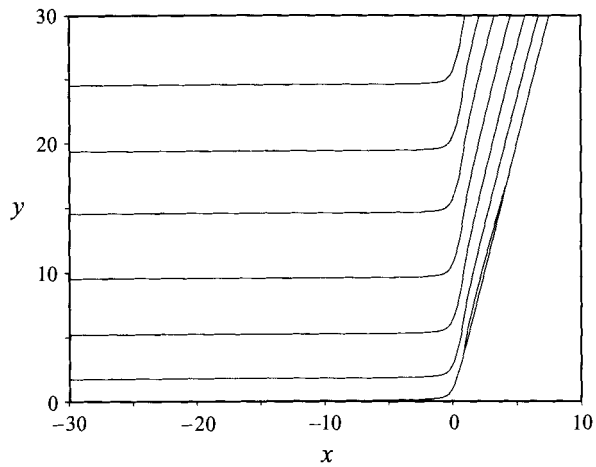

FIGURE 9. Streamlines for $\alpha = 4$ and $S\mathscr{L} = -12.5$

The effects of supercritical wall cooling on the recirculating region itself are displayed in the results for pressure and wall shear in figures 3–6 and the streamline plots shown in figures 7–9. The primary features observed are a progressive downstream shift in the point of separation toward the corner and an overall reduction in the streamwise and normal extents of the recirculating-flow region. Indeed, for all ramp angles considered where separation occurs in the non-cold wall case ($\alpha = 2.0$, 3.0, 4.0 and 5.0), separation was ultimately eliminated by sufficient wall cooling. Figures 5*a* and 6*a* also show that increased wall cooling decreases the value of the pressure plateau in the region of recirculating flow. Comparison of figure 7 for $\alpha = 3.0$ with figure 4 of Cassel *et al.* (1995) for the non-cold wall case shows the effects of wall cooling on the streamlines. Without wall cooling, the flow passes smoothly over the recirculating-flow region; however, with wall cooling, the streamlines experience an increasingly abrupt change in direction just upstream of separation as the wall cooling is increased until separation is completely suppressed and the streamlines again become smooth. This is also shown in the streamline plots of figure 8 for a series of cases with $\alpha = 5.0$. In addition, figure 8 shows that for relatively high ramp angles, there is a dramatic thinning of the recirculation zone downstream of the corner as the wall is cooled, but at the same time there is little change in the streamwise location of reattachment. Note that figure 8(*a*) shows the streamlines for a case involving secondary separation at the corner in which a small recirculating-flow region forms within the primary reversed-flow region. Observe that the streamlines in the primary recirculating-flow region rise abruptly as they pass over the secondary separation. This secondary separation is eliminated as the wall cooling is increased, in the same way that the primary reversed-flow region vanishes. It may be noted that as the level of wall cooling is increased, the separation region thins and moves up onto the ramp for a given value of α. This phenomenon is illustrated in figure 9, where the streamlines for an example with $\alpha = 4.0$ and $S\mathscr{L} = -12.5$ are shown; here the separation point is located on the ramp downstream of the corner, and the recirculating flow is completely contained on the ramp. This trend is consistent with the theory of strong wall cooling of supercritical boundary layers described by Kerimbekov *et al.* (1994). Many other cases were found to have separation occurring downstream of the corner, but as observed in figure 9, the recirculating flow region becomes very thin, and it

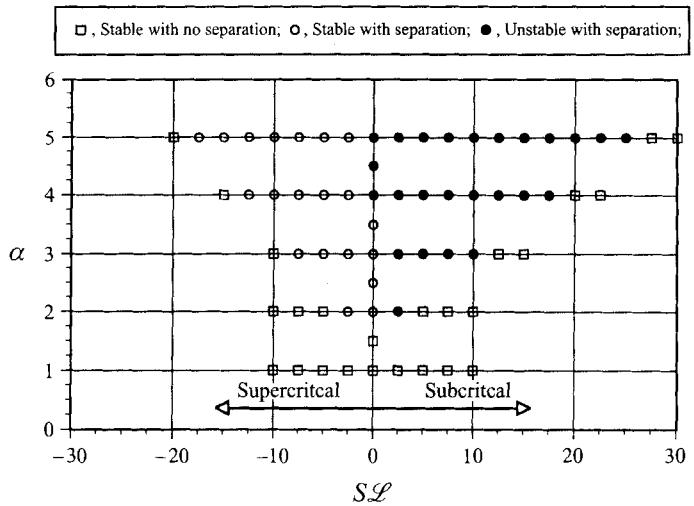

FIGURE 10. Summary of separation and stability characteristics for flows computed with various ramp angles α and levels of wall cooling $S\mathscr{L}$.

is progressively more difficult to plot the separation streamline as the wall cooling is increased.

The separation and stability characteristics of all the cases shown in this work and Cassel *et al.* (1995) are summarized in figure 10. The non-cold wall results of Cassel *et al.* (1995) are shown along the line $S\mathscr{L} = 0$, while wall cooling cases in the supercritical and subcritical regimes are shown for $S\mathscr{L} < 0$ and $S\mathscr{L} > 0$, respectively. As discussed by Cassel *et al.* (1995), separation occurs in cases without wall cooling for $\alpha \geqslant 1.9$ and becomes unstable for $\alpha \geqslant 3.9$. It may be observed from figure 10 that as the ramp angle is increased, a progressively larger range of $S\mathscr{L}$ (both subcritical and supercritical) exists for which separation occurs. However, for both subcritical and supercritical boundary layers, separation is eliminated with sufficient wall cooling (at least for $\alpha \leqslant 5.0$). Wall cooling in a supercritical boundary layer appears to be more effective in suppressing separation. For example, for $\alpha = 5.0$ separation is eliminated for $S\mathscr{L} \leqslant -20.0$ in the supercritical regime but values of $S\mathscr{L} \geqslant 27.5$ are required in the subcritical regime.

The effect of wall cooling on stability is more dramatic. For supercritical boundary layers, wall cooling has a strong stabilizing effect while for subcritical boundary layers, it is strongly destabilizing. From figure 10 it can be seen that all supercritical cases computed remained stable; in contrast, all subcritical cases involving separation became unstable, and those where separation did not occur remained stable. The stabilizing effect of wall cooling on supercritical boundary layers in two-dimensional flow has been observed experimentally by Lewis *et al.* (1968) who considered the supersonic flow over compression ramps; the same effect is also discussed in the review by Stetson & Kimmel (1992) of the stability characteristics of hypersonic boundary layers.

Next it is of interest to confirm the scalings (3.2) of Kerimbekov *et al.* (1994) for the strong wall cooling case. This was carried out here through comparison of the present results for $S|\mathscr{L}|$ large, but $O(1)$, with the theoretical results of Kerimbekov *et al.* (1994). Recall from equations (3.2*a*) and (3.2*e*) that the strong wall cooling variables are related to the current variables by $\bar{x} = N^{-3/4}x$, $\bar{p} = N^{-1/2}p$ and $\bar{\alpha} = N^{-1/2}\alpha$,

Ramp angle α	Subcritical $S\mathscr{L}$	Supercritical $S\mathscr{L}$
1.0	10.0	-10.0
2.0	10.0	-10.0
3.0	15.0	-10.0
4.0	22.5	-15.0
5.0	30.0	-20.0

TABLE 1. Wall cooling values $S\mathscr{L}$ used with subcritical and supercritical regimes for each ramp angle α for comparison in figure 11 of numerical results with the strong wall cooling theory of Kerimbekov *et al.* (1994).

respectively. For $N = [S|\mathscr{L}|]^{4/3} \gg 1$, the leading-order pressure distribution for the compression ramp is given by equations (3.9) and (3.10) for the supercritical and subcritical cases, respectively. In order to compare the numerical results obtained here with these analytical results, the computed pressure distributions for $\alpha = 1.0$, 2.0, 3.0, 4.0 and 5.0 for both the subcritical and supercritical cases were replotted in terms of the scaled variables and compared with the analytical results. Note that since the scales for $\bar{p}$ and $\bar{\alpha}$ are the same, the pressure distributions defined by equations (3.9) and (3.10) are the same in terms of p and α. For each ramp angle, the subcritical and supercritical case computed with the largest level of wall cooling (see figure 10) was scaled in terms of $\bar{x}$ and compared to the analytical results (3.9) and (3.10). The wall cooling parameters used for each ramp angle are shown in table 1, and the comparisons are shown in figure 11(*a*) for the subcritical regime and figure (11*b*) for the supercritical regime. Observe that the agreement is very good even for the relatively small values of $S|\mathscr{L}|$ used in the numerical calculations (see table 1). Note that the small discrepancies near $\bar{x} = 0$ are associated with the slight rounding of the corner used in the numerical calculations.

In addition to the above comparisons of the pressure distributions, a series of calculations were carried out for the supercritical case in order to determine when separation first appears as $S|\mathscr{L}|$ is increased. This was done by determining the ramp angle α_0 and streamwise location x_0 at which separation first appears for various levels of wall cooling. For each value of $-S\mathscr{L}$ in increments of 5.0, a series of calculations were carried out with increasing values of the ramp angle α until a small separation bubble first formed on the surface. This ramp angle α_0 and the streamwise location x_0 at which it occurs for each value of $-S\mathscr{L}$ is shown in figure 12. These results were obtained on meshes defined by $I = 201$, $J = 101$, $a = b = 10.0$ for $S|\mathscr{L}| \leqslant 30.0$ and $a = b = 20.0$ for $S|\mathscr{L}| \geqslant 35.0$. An expanded mesh was used for higher levels of wall cooling because as $-S\mathscr{L}$ is increased, separation moves downstream and greater resolution is necessary in regions remote from the corner. As the degree of wall cooling is increased, figure 12 shows that the critical ramp angle required for separation increases. In addition, the streamwise location where separation appears moves well downstream of the corner as predicted by the theory of Kerimbekov *et al.* (1994). This procedure was terminated at $S\mathscr{L} = -45.0$ because as separation moves downstream of the corner for increased wall cooling, it becomes increasingly difficult to obtain accurate numerical solutions using the present algorithm, which packs points near the corner at the expense of resolution upstream and downstream.

The results of Kerimbekov *et al.* (1994) show that for $N \gg 1$, the critical ramp angle and the location at which separation first occurs in terms of the scaled variables

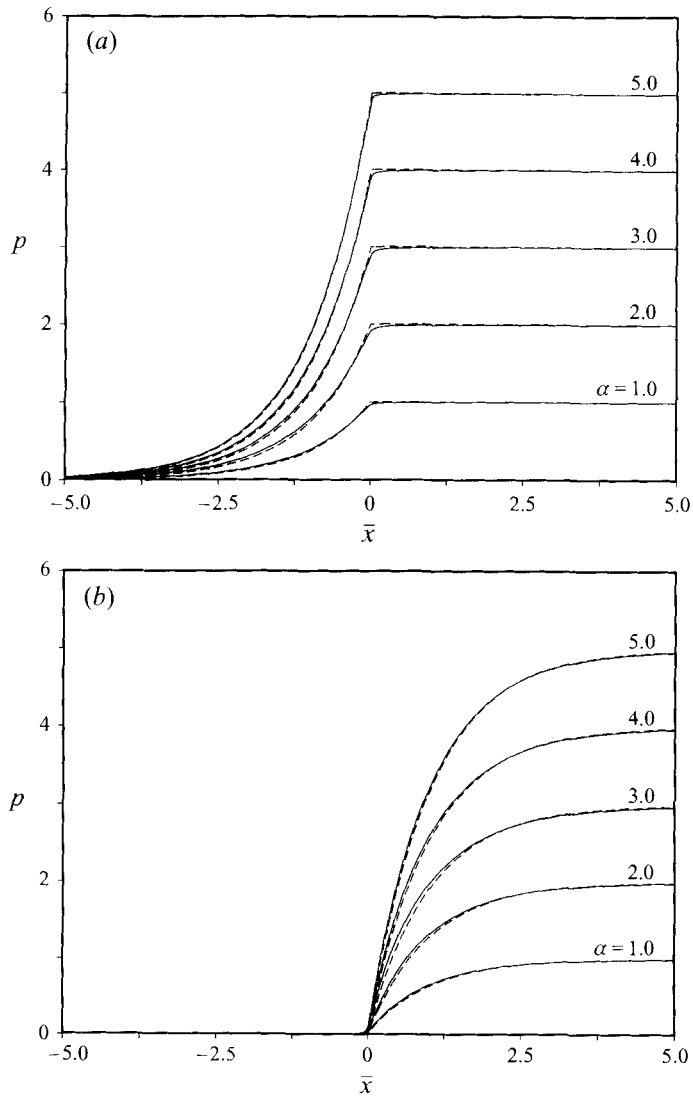

FIGURE 11. Comparison of pressure distributions from numerical results (—) for cases given in table 1 with analytical results (- - - -) for the strong wall cooling case. (*a*) Subcritical boundary layer, (*b*) supercritical boundary layer.

(3.2) are $\bar{\alpha}_0 = 0.7548$ and $\bar{x}_0 = 0.5$, respectively. In order to confirm these values, the incipient separation results shown in figure 12 are presented in figure 13 in terms of the scaled variables $\bar{\alpha}$ and $\bar{x}$. Again, accurate results for larger values of $-S\mathscr{L}$ could not be obtained from the present algorithm, and it is evident from figure 13*b* that the results for x_0 when $S\mathscr{L} = -45.0$ may be questionable. However, as $S|\mathscr{L}|$ increases, it does appear that the numerical results for $\bar{\alpha}_0$ and $\bar{x}_0$ are tending to the critical values for large N determined by Kerimbekov *et al.* (1994). Therefore, the present numerical investigation appears to confirm the scalings (3.2) for the strong wall cooling case. Particularly strong evidence of this is given by the comparisons of the pressure distributions in figures 11(*a*) and 11(*b*).

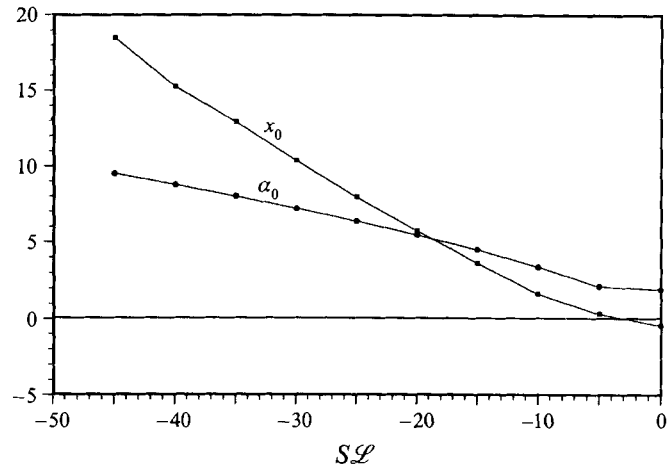

FIGURE 12. Critical ramp angle α_0 at which incipient separation of a supercritical boundary layer occurs for various values of wall cooling and the streamwise location x_0 where it appears.

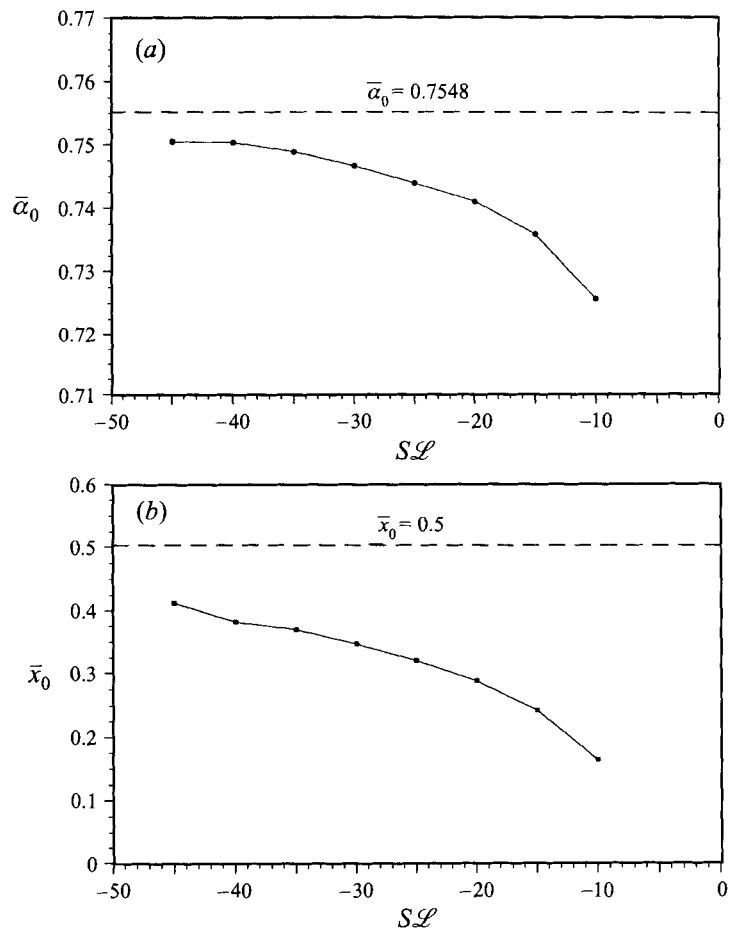

FIGURE 13. Incipient separation results for figure 12 shown in terms of strong wall cooling variables; critical values from Kerimbekov *et al.* (1994) are shown for comparison. (*a*) Critical ramp angle $\bar{\alpha}_0$ at which separation first occurs, (*b*) streamwise location $\bar{x}_0$ where incipent separation appears.

7. Discussion

A general algorithm has been implemented for calculation of the hypersonic triple deck on a cold wall. The algorithm applies for general surface shapes on the triple-deck scale, but it has been used here to compute the flow over the compression ramp geometry with various reduced ramp angles α and levels of wall cooling $S\mathscr{L}$. Available steady-state solutions were calculated as the large-time limit of unsteady calculations.

Tutty & Cowley (1986) show that for the non-cold wall case (or equivalently the supersonic case), Rayleigh's and Fjørtoft's criteria are necessary conditions for a high-wavenumber instability. For the cold wall case, however, no analogous conditions could be determined which were particularly useful in identifying an instability. A linear stability analysis does produce a stability condition which provides a necessary and sufficient criterion for the occurrence of a high-wavenumber inviscid instability for cases both with and without wall cooling, but this condition proved difficult to evaluate accurately for the flow over the compression ramp (see Cassel *et al.* 1995).

Numerical solutions were determined for various ramp angles without wall cooling ($S\mathscr{L} = 0$) by Cassel *et al.* (1995), and separation was found to occur near the corner for ramp angles $\alpha \geqslant 1.9$ for the slightly rounded corner geometry used here. The recirculating-flow region grows in streamwise and normal extent, and a pressure plateau forms in the pressure distribution as the ramp angle is increased beyond this value. For ramp angles with $\alpha \geqslant 3.9$, a high-frequency instability develops in the form of a wave packet which remains stationary near the corner once sufficiently refined grids were used. The instability has high frequencies and short wavelengths, and for this reason it is highly mesh dependent. In addition, the occurrence of this instability in the numerical computations was shown to be consistent with Rayleigh's and Fjørtoft's criteria.

Here, wall cooling was found to have a significant effect upon both the separation and stability characteristics of the flow. Wall cooling of subcritical boundary layers has a strong destabilizing effect, while for supercritical flows, it has a strong stabilizing effect. In fact, every case considered involving supercritical boundary layers for the ramp angles investigated (up to $\alpha = 5.0$) remained stable. On the other hand, every case computed with subcritical flow which involved separation became unstable, while those without separation remained stable.

The location and extent of the recirculating flow is also affected significantly by wall cooling, and sufficient wall cooling of both subcritical and supercritical boundary layers can eliminate separation altogether. For the supercritical cases, increasing the level of wall cooling reduces the size of the recirculating-flow region, shifts the separation point downstream, and generally reduces upstream influence. Conversely, wall cooling of subcritical flows reduces downstream influence; these trends continue until, in the limit of large Neiland number N, no disturbances associated with the ramp are permitted upstream of the corner for supercritical flow or downstream of the corner for subcritical flow.

Finally, the present results verify the strong wall cooling theory of Kerimbekov *et al.* (1994) which is valid for large N. The pressure distributions obtained numerically for large but finite $S|\mathscr{L}|$ compared well (even for relatively small $S|\mathscr{L}|$) with the analytical results valid for $N \to \infty$ for the leading-order pressure in both the subcritical and supercritical cases. In addition, good agreement was found with the incipient separation results of Kerimbekov *et al.* (1994) for the supercritical case. As $-S\mathscr{L}$ is increased, it was shown that the ramp angle at which separation first occurs also

increases, and the separation point moves well downstream of the corner. When scaled according to the strong wall cooling variables, the present results tend toward the critical values determined by Kerimbekov *et al.* (1994) in the limit $-S\mathscr{L} \to \infty$. Therefore, the present results provide a smooth bridge from the classical supersonic (and hypersonic) triple-deck problem to the strongly cooled wall results of Kerimbekov *et al.* (1994).

This work was supported by NASA Lewis Research Center under Grant No. NAG3-1578. K.W.C. was supported by a National Defense Science and Engineering Graduate Fellowship. A.I.R. was supported in part by the Air Force Office of Scientific Research under Contract No. F49620-93-1-0130.

Appendix A

The present study is based on the original approach of Neiland (1973) and differs in some respects from the more recent formulation of Brown *et al.* (1990) who, for example, use the Dorodnitsyn variable to measure a density-weighted normal distance from the wall. As noted by Brown *et al.* (1990), some aspects of the two approaches are not easily compared. Nevertheless, a brief comparison of some important features is given here.

Brown *et al.* (1990) derive an interaction law of the form $p = -\sigma(\partial A/\partial x + v\partial p/\partial x)$, which is a relation also developed by Brown, Stewartson & Williams (1975) somewhat after the interaction relation (2.9) was given by Neiland (1973). If $y = f(x)$ denotes the wall contour, the form of the interaction law after a Prandtl transposition is

$$p = -\sigma\left(\frac{\mathrm{d}A}{\mathrm{d}x} + \frac{\mathrm{d}f}{\mathrm{d}x} + v\frac{\mathrm{d}p}{\mathrm{d}x}\right), \tag{A 1}$$

which is clearly similar to equation (2.9). In equation (A 1), σ and v are parameters which Brown *et al.* (1990) show satisfy the relation

$$v^4\sigma = \left(\frac{T_w^*}{T_w}\right)^{4n+2}, \tag{A 2}$$

where T_w is the wall temperature, and T_w^* is a characteristic temperature which is $O(\chi^{1/(4n+2)})$; both theories agree that the important characteristic temperature has this order of magnitude. The triple-deck problem formulated by Brown *et al.* (1990) contains five parameters (including σ and v), but since there are only four connecting relations, they argue that one parameter may be specified arbitrarily. Brown *et al.* (1990) first set $\sigma = 1$ and identify two situations for which $v \ll 1$ and $v = O(1)$. For $\sigma = 1$ the two interaction laws (A 1) and (2.9) are identical if $v = -S\mathscr{L}$. Note that although Brown *et al.* (1990) consider only the case $v > 0$, Neiland (1973) (see also Kerimbekov *et al.* 1994) has shown that $S > 0$, while $\mathscr{L}$ may be either negative or positive, corresponding to the present definitions of supercritical and subcritical flow, respectively. Brown *et al.* (1990) refer to the cases $v \ll 1$ and $v = O(1)$ as supercritical and transcritical, respectively; these cases have been described here as temperature regimes 1 and 2, corresponding to moderate wall temperatures and moderate wall cooling, respectively. The former situation is described by the classical Ackeret interaction law, while the latter case is characterized by a significant contribution in the interaction law (2.9) or (A 1) due to the main deck.

Calculations were carried out in the present study for the same parameters considered by Brown *et al.* (1990) in regime 2 for compression ramp flow and essentially the

same results were obtained. It is worthwhile to note that the numerical techniques in both studies are substantially different. Brown *et al.* (1990) assume that the motion in the interaction region is steady and do not investigate the question of stability. Their numerical method employs an iterative solution of the steady equations and requires the inversion of large matrices associated with the finite difference approximations; this approach necessarily places significant restrictions on the number of mesh points that can be used. In contrast, the time-dependent evolution of the flow was of interest in the present study, and possible steady solutions were sought as the potential limit of an unsteady calculation. Because the numerical method does not involve the inversion of large matrices, calculations could be carried out on grids that are more highly refined than in previous studies. The results show that, depending on the value of S, $\mathscr{L}$ and the scaled ramp angle α, the flow may be either stable or unstable. For stable flows, the solutions approach those of Brown *et al.* (1990).

It is the strong wall cooling case (regime 3) where the two theories disagree. In this situation, the right-side of equation (A 2) becomes large but, as Brown *et al.* (1990) discuss, their expansions become disordered in the limit process $\sigma = 1$, $v \to \infty$. Instead they consider the limit process $v = 1$ and $\sigma \to \infty$. However there is a difficulty with the latter limit since calculated values of the pressure do not approach a plateau downstream (see Appendix B of Kerimbekov *et al.* 1994 for an explanantion). In contrast, the present solutions exhibit the proper behaviour as $S|\mathscr{L}|$ becomes large and blend smoothly into the analytical results obtained in the limit $N = (S|\mathscr{L}|)^{4/3} \to \infty$ by Kerimbekov *et al.* (1994).

REFERENCES

Brown, S. N., Cheng, H. K. & Lee, C. J. 1990 Inviscid-viscous interaction on triple-deck scales in a hypersonic flow with strong wall cooling. *J. Fluid Mech.* **220**, 309–337.

Brown, S. N., Stewartson, K. & Williams, P. G. 1975 Hypersonic self-induced separation. *Phys. Fluids* **18**, 633–639.

Burggraf, O. R. & Duck. P. W. 1982 Spectral computation of triple-deck flows. *Proc. symp. on Numerical and Physical Aspects of Aerodynamic Flows.* (ed. T. Cebeci), pp. 145–158. Springer.

Cassel, K. W. 1993 The effect of interaction on boundary-layer separation and breakdown. PhD thesis, Lehigh University, Bethlehem, Pennsylvania.

Cassel, K. W., Ruban, A. I. & Walker, J. D. A. 1995 An instability in supersonic boundary-layer flow over a compression ramp. *J. Fluid Mech.* **300**, 265–285.

Duck, P. W. 1987 Unsteady triple-deck flows leading to instabilities. *Proc. on Boundary-Layer Separation, IUTAM Symp.* (ed. F. T. Smith & S. N. Brown), pp. 297–312. Springer.

Goldstein, S. 1948 On laminar boundary-layer flow near a point of separation. *Q. J. Mech. Appl. Maths* **1**, 43–69.

Kerimbekov, R. M., Ruban, A. I. & Walker, J. D. A. 1994 Hypersonic boundary-layer separation on a cold wall. *J. Fluid Mech.* **274**, 163–195.

Lewis, J. E., Kubota, T. & Lees, L. 1968 Experimental investigation of supersonic laminar, two-dimensional boundary-layer separation in a compression corner with and without cooling. *AIAA J.* **6**, 7–14.

Neiland, V. Ya. 1969 On the theory of laminar boundary-layer separation in supersonic flow. *Izv. Akad. Nauk SSSR, Mekh. Zhid. Gaza*, No. 4, 53–57.

Neiland, V. Ya. 1973 Peculiarities of boundary-layer separation on a cooled body and its interaction with a hypersonic flow. *Izv. Akad. Nauk SSSR, Mekh. Zhid. Gaza*, No. 6, 99–109.

Neiland, V. Ya. 1987 Peculiarities of interaction and separation of the transcritical boundary layer. *Uch. Zap. TsAGI.* **18** (2), 30–45.

Neiland, V. Ya. & Socolov, L. A. 1975 On the asymptotic theory of incipient separation in compression ramp hypersonic flow on cooled body for a weak hypersonic interaction regime. *Uchen. Zap. TsAGI* **6**, No. 3, 25–34.

RIZZETTA, D. P., BURGGRAF, O. R. & JENSON, R. 1978 Triple-deck solutions for viscous supersonic and hypersonic flow past corners. *J. Fluid Mech.* **89**, 535–552.

RUBAN, A. I. 1978 Numerical solution of the local asymptotic problem of the unsteady separation of a laminar boundary layer in a supersonic flow. *USSR Comput. Maths Phys.* **18**, 175–187.

RUBAN, A. I. 1981 Singular solution for boundary-layer equations with continuous extension downstream of zero skin friction point. *Izv. Akad. Nauk. SSSR. Mekh. Zhid. Gaza* No. 6, 42–52.

RUBAN, A. I. 1982 Asymptotic theory for short separation bubbles on the leading edge of thin airfoils. *Izv. Akad. Nauk. SSSR. Mekh. Zhid. Gaza* No. 1, 42–51.

SEDDOUGUI, S. O., BOWLES, R. I. & SMITH, F. T. 1991 Surface cooling effects on compressible boundary-layer instability and on upstream influence. *Eur. J. Mech.* B/*Fluids* **10**, 117–145.

SMITH, F. T. & DANIELS, P. G. 1981 Removal of Goldstein's singularity at separation in flow past obstacles in wall layers. *J. Fluid Mech.* **110**, 1–37.

SMITH, F. T. & KHORRAMI, A. F. 1991 The interactive breakdown in supersonic ramp flow. *J. Fluid Mech.* **224**, 197–215.

STETSON, K. F. & KIMMEL, R. L. 1992 On hypersonic boundary-layer stability. *AIAA Paper* 92-0737.

STEWARTSON, K., SMITH, F. T. & KAUPS, K. 1982 Marginal separation. *Stud. Appl. Maths* **67**, 45–61.

STEWARTSON, K. & WILLIAMS, P. G. 1969 Self-induced separation. *Proc. R. Soc. Lond.* A **312**, 181–206.

TOWEND, L. H. 1991 Research and design for hypersonic aircraft. *Phil. Trans. R. Soc. Lond.* A **335**, 201–224.

TUTTY, O. R. & COWLEY, S. J. 1986 On the stability and the numerical solution of the unsteady interactive boundary-layer separation. *J. Fluid Mech.* **168**, 431–456.

WALBERG, G. D. 1991 Hypersonic flight experience. *Phil. Trans. R. Soc. Lond.* A **335**, 91–119.

ZHIKHAREV, C. N. 1993 Separation phenomenon in a hypersonic flow with strong wall cooling: subcritical regime. *Theoret. Comput. Fluid Dyn.* **4**, 209–226.